2.8 Transverse Emittance Preserving Arc Compressor

Simone Di Mitri
Elettra – Sincrotrone Trieste S.C.p.A., S.S.14 km163,5 in Area Science Park,
Trieste, I-34149
Mail to: simone.dimitri@elettra.eu

2.8.1 Introduction

The advent of short electron bunches in high brightness linear accelerators has raised the awareness of the accelerator community to the degradation of the beam transverse emittance by coherent synchrotron radiation (CSR) emitted in magnetic insertions for bunch length compression. Beam optics control has been proposed to mitigate that CSR effect. In this article, we follow the findings presented in [1,2] in order to review the linear optics approach in a periodic, locally achromatic arc compressor. We study the dependence of the CSR-perturbed emittance on beam optical functions, mean energy, and bunch charge. The analytical expectations are compared with particle tracking runs. We thereby identify a range of parameters that allows feasibility of an arc compressor for driving, for example, a free electron laser or a linear collider. Application to a recirculating linac-based free electron laser is discussed with some detail.

2.8.2 CSR Kicks in a Linear Optics Model

2.8.2.1 *Theoretical Background*

Linear optics analysis in the presence of CSR kicks was introduced in [3]. It considers the effect of CSR on the particle transverse motion through the first order energy dispersion only. This may be justified if the kick (i.e., change in particle's transverse momentum) provided by the radial forces associate to the CSR field [4], is much smaller than the CSR-induced chromatic kick. This is actually the case for the compressed beam parameters considered in this article, as well as for many realistic cases of ultraviolet and x-ray free electron laser (FEL) linac drivers. The effect of radiation shielding by the vacuum chamber [5,6] can be neglected as long as the wavelength at which CSR starts being suppressed, $\lambda \geq 2g(g/\rho)^{1/2}$ (g is the vacuum chamber gap and ρ the bending radius), is longer than the compressed electron bunch length, σ_z. In the present article, we will consider practical situations in which $\lambda \geq 1$mm and $\sigma_z \leq 0.1$ mm. Particles' motion is linear in the particle betatron coordinates, which implies preservation of the particle Courant-Snyder (C-S) invariant and of the beam rms emittance in between consecutive kicks. This assumption may be invalidated in practice by geometric and chromatic optical aberrations, which may affect the rms emittance in the presence of strong quadrupole and sextupole gradients, and large energy spread. Finally, the CSR chromatic kick is concentrated in the middle of the dipole magnet, and in fact the dipole is treated as a thin lens. The latter point was shown in [7] to be a limitation for the evaluation of the optics solution that minimizes the CSR emittance, and the analysis was extended in that work to take into account the evolution of the CSR wakefield along the dipole magnet:

$$\begin{pmatrix} \Delta x_{CSR} \\ \Delta x'_{CSR} \end{pmatrix} = \begin{pmatrix} \rho^{4/3} k(\theta - \sin(\theta)) \\ \rho^{1/3} k(1 - \cos(\theta)) \end{pmatrix} = \delta_{CSR} \begin{pmatrix} \rho\left(1 - \dfrac{\sin(\theta)}{\theta}\right) \\ \dfrac{1-\cos(\theta)}{\theta} \end{pmatrix} \tag{1}$$

We adopted in Eq.1 the same notation than in [7], where ρ is the dipole bending radius, $\delta_{CSR}=\rho^{1/3}k\theta$ is the particle relative energy deviation induced by CSR after a bending angle θ, and $k=0.2459 r_e Q/(e\gamma\sigma_z^{4/3})$ is the CSR kick factor, which is function of the number of electrons per bunch Q/e, the electron classical radius r_e and the energy Lorentz factor γ. k relates the transverse CSR effect to the rms bunch length σ_z, and applies to a Gaussian longitudinal charge distribution emitting CSR in the steady-state regime. In general, a different dependence of k on σ_z could be considered for different current profiles [8].

Eq.1 can be used to evaluate the single particle C-S invariant along an arbitrary beamline: the effect of a CSR kick is added with the prescription $x \rightarrow x + \Delta x_{CSR}$, $x' \rightarrow x' + \Delta x'_{CSR}$ [3]. The particle coordinates are then propagated through the beamline, in the absence of kicks, with the standard transfer matrix given in terms of the beamline Twiss parameters β and α (in the plane of interest):

$$\begin{pmatrix} x \\ x' \end{pmatrix}_{s_1} = \begin{pmatrix} \sqrt{\dfrac{\beta_1}{\beta_0}}(\cos\Delta\mu + \alpha_0 \sin\Delta\mu) & \sqrt{\beta_0\beta_1}\sin\Delta\mu \\ \dfrac{\alpha_0 - \alpha_1}{\sqrt{\beta_0\beta_1}}\cos\Delta\mu - \dfrac{1+\alpha_0\alpha_1}{\sqrt{\beta_0\beta_1}}\sin\Delta\mu & \sqrt{\dfrac{\beta_0}{\beta_1}}(\cos\Delta\mu - \alpha_1\sin\Delta\mu) \end{pmatrix} \begin{pmatrix} x \\ x' \end{pmatrix}_{s_0} \tag{2}$$

In Eq.2, $\Delta\mu$ is the betatron phase advance between the longitudinal location s_0 and s_1 in the beamline. The single particle invariant is $J = \beta x'^2 + 2\alpha x x' + \left(\dfrac{1+\alpha^2}{\beta}\right)x^2$.

The more accurate expression for the CSR kick cumulated over a non-zero dipole length, see Eq.1, was borrowed in [1] to extend the revised optics balance to the case of varying bunch length in an arc compressor; we recall that treatment in the next Section. Clearly, the constraint of identical CSR kicks (in module) at different dipole magnets falls short there, because the bunch length is compressed along the line.

2.8.2.2 *Periodic and Locally Achromatic Arc Compressor*

The periodic, achromatic 180 deg arc compressor introduced in [1] is made of 6 identical DBA cells. The single DBA magnetic lattice and its periodic optics solution is shown in Fig.1. At first, we focus on the single DBA cell and write down the particle coordinates at the end of the second dipole:

$$\begin{cases} x_3 = -\rho^{4/3}k_1(\theta C_\theta - 2S_\theta) + \rho^{4/3}k_2(\theta C_\theta - 2S_\theta) \\ x'_3 = -\rho^{1/3}k_1\theta S_\theta - \rho^{1/3}k_2\theta S_\theta - \dfrac{2\alpha_2}{\beta_2}\rho^{4/3}k_1(\theta C_\theta - 2S_\theta), \\ \delta_3 = \rho^{1/3}k_1\theta + \rho^{1/3}k_2\theta \end{cases} \tag{3}$$

where $C_\theta=\cos(\theta/2)$ and $S_\theta=\sin(\theta/2)$, k_1 (k_2) is the CSR kick factor in the first (second) dipole, and the subscript "2" of the Twiss parameters refers to the middle point of the second dipole of the DBA. We thus calculate the expression of the single particle C-S

invariant at the end of the second dipole magnet for arbitrary Twiss parameters in the dipoles, by considering a dependence of the CSR kick factor on the rms bunch length $k \sim 1/\sigma_z^{4/3}$, so that $k_2 = k_1 \times C^{4/3}$. Doing so, we consider: i) optics symmetry w.r.t. the DBA central axis, which implies π betatron phase advance (in the bending plane) between the dipoles [9], and ii) expand the trigonometric terms up to the third order in the bending angle, $\theta << 1$ [1]:

$$\begin{aligned} J_3 &= \beta_2 x_3'^2 + 2\alpha_2 x_3 x_3' + \left(\frac{1+\alpha_2^2}{\beta_2}\right) x_3^2 = \\ &\cong \left(\frac{k_1 \rho^{1/3}\theta^2}{2}\right)^2 \left[\beta_2 \left(C^{4/3}+1\right)^2 + \frac{1}{\beta_2}\left(\frac{l_b}{6}\right)^2 \left[\left(C^{4/3}-1\right)^2 + \alpha_2^2\left(C^{4/3}-3\right)^2\right] + 2\alpha_2 \left(\frac{l_b}{6}\right)\left(C^{4/3}+1\right)\left(C^{4/3}-3\right)\right] \end{aligned} \tag{4}$$

In Eq.4, $l_b = \rho\theta$ is the dipole arclength, and C the *local* linear compression factor. An inspection of Eq.4 shows that the invariant can be made exactly zero *only* for C = 1. To show this, we point out that minimization of J_3 requires [2]:

$$\begin{aligned} \left(\frac{dJ_3}{d\alpha_2}\right)_{\beta_2} &= \left(\frac{k_1 \rho^{1/3}\theta^2}{2}\right)^2 \left[\frac{2\alpha_2}{\beta_2}\left(\frac{l_b}{6}\right)^2 \left(C^{4/3}-3\right)^2 + 2\left(\frac{l_b}{6}\right)\left(C^{4/3}+1\right)\left(C^{4/3}-3\right)\right] \equiv 0 \\ \left(\frac{dJ_3}{d\beta_2}\right)_{\alpha_2} &= \left(\frac{k_1 \rho^{1/3}\theta^2}{2}\right)^2 \left[\left(C^{4/3}+1\right)^2 - \frac{1}{\beta_2}\left(\frac{l_b}{6}\right)^2 \left[\left(C^{4/3}-1\right)^2 + \alpha_2^2\left(C^{4/3}-3\right)^2\right]\right] \equiv 0, \end{aligned} \tag{5}$$

from which we get:

$$\begin{aligned} \alpha_{2,opt} &= -\frac{\beta_2}{\left(\frac{l_b}{6}\right)} \frac{\left(C^{4/3}+1\right)}{\left|C^{4/3}-3\right|} \\ \beta_{2,opt} &= \left(\frac{l_b}{6}\right) \frac{\sqrt{\left(C^{4/3}-1\right)^2 + \alpha_2^2\left(C^{4/3}-3\right)^2}}{\left(C^{4/3}+1\right)} \end{aligned} \tag{6}$$

By substituting $\alpha_{2,opt}$ into the expression for $\beta_{2,opt}$ or vice versa, we find that the derived expression is satisfied for C=1 only, in which case we obtain $\alpha_{2,opt}(C=1) = -\frac{6\beta_{2,opt}}{l_b}$. This is the solution for the non-compressed beam in a symmetric DBA already found in [7]. We observe that $\alpha_{2,opt}$ is negative for any C, which in our case corresponds to a diverging (converging) beam size in the second (first) dipole magnet, and that it is always different from zero. In other words, a solution with $\alpha_2 = 0$ like that adopted in [1] does not minimize J_3 in *absolute* sense, although it may be practical from the optics design point of view. As expected, Eq.6 reduces to Eq.5 in [1] for $\alpha_2 = 0$.

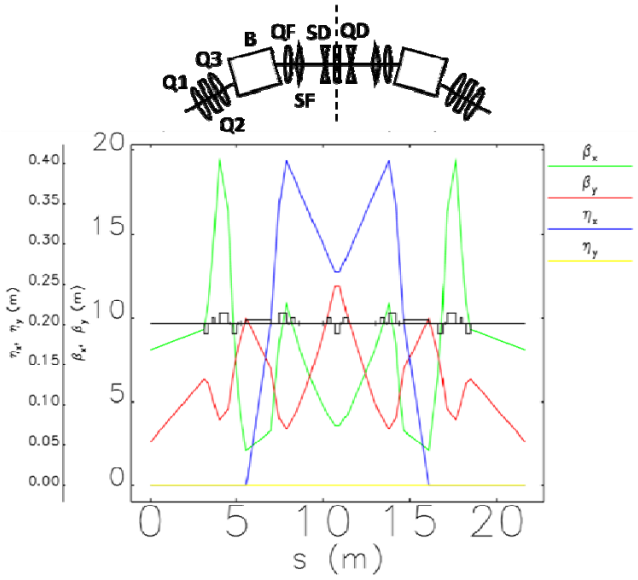

Figure 1: Sketch, not to scale, of the magnetic lattice of a DBA cell of the arc compressor (top), and periodic linear optics functions through the cell. Dipole magnets (B), focusing (QF, Q1 and Q3) and defocusing (QD, Q2) quadrupole magnets, focusing (SF) and defocusing sextupole magnets (SD) are labelled. The geometry and the magnets' arrangement is symmetric with respect to the middle axis (dashed line). Copyright of Elsevier [2].

It is quite common to have $\alpha_1 = \alpha_2 = 0$ in a rather compact and symmetric DBA design, such as that shown in Fig.1. In the following, we will keep it as a constraint on the optics design, and will study how β_2 should be tuned along the DBA according to the local value of the bunch length compression factor, C. That is defined by $C=1/|1+hR_{56}|$, where R_{56} is the transfer matrix element of the DBA cell, identical in all cells, and h is the incoming linear energy chirp, h=dE/(Edz). Bunch length compression is achieved as far as the energy spread correlated along the bunch, typically imparted to the beam by an upstream RF section running far from the accelerating crest, is much larger than the uncorrelated energy spread. In that case we can also write $h \approx \sigma_{\delta,0}/\sigma_{z,0}$, with $\sigma_{\delta,0}$ the initial rms value of the beam relative energy spread, and $\sigma_{z,0}$ the rms value of the initial bunch length. While σ_δ does not change substantially during the compression process, σ_z clearly shortens with C, that is h increases along the arc, and C so does. Eventually, the local compression factor, C^{loc}, and that cumulated through the lattice, C^{tot}, depends on the cell number:

$$C_i^{loc} = \frac{1}{|1 + C_{i-1} h_{i-1} R_{56}|}, \quad i = 1,...,6$$
$$C_j^{tot} = \prod_{i=1}^{j} \frac{1}{|1 + C_{i-1} h_{i-1} R_{56}|}, \quad j = 1,...,6 \qquad (7)$$

C^{tot} grows nonlinearly with the s-coordinate along the arc, and, according to Eq.6, β_2 should be tuned accordingly in each DBA, in order to optimally minimize the CSR-induced emittance growth (henceforth simply "CSR emittance"). In particular, β_2 should be made larger in the dipoles of the last DBA cells. Since the CSR effect is larger for shorter bunches, we might be allowed to relax the condition on β_2 in the first

few cells, where the bunch is longer, while ensuring optimum optics tuning in the last ones. The CSR emittance at the end of the arc is the result of the cumulative effect of CSR kicks in each cell. We assume that the CSR emittance in each cell sums in quadrature to the total emittance of the incoming beam, where the normalized emittance in the *i-th* cell is estimated by means of the "sigma matrix formalism" [10] and it reads:

$$\varepsilon_{n,i} \cong \sqrt{\varepsilon_{n,i-1}^2 + \varepsilon_{n,i-1}\gamma_i J_i} \tag{8}$$

γ_i is the usual relativistic Lorenz factor for the beam energy, J_i was defined in Eq.4 and we have to evaluate it with the prescription $C=C_i^{loc}$ according to Eq.7. Figure 2-left plot shows C_i^{loc}, $\beta_{x,opt}$ and γJ_i along the arc, for the beam parameters listed in Tab.1 (henceforth, β_x always refers to the betatron function in the dipole magnets). Figure 2-right plot compares J_i evaluated for $\beta_{x,opt}$ as in the left plot, to that for an identical value of β_x in all the dipoles. The CSR emittance is dominated by the CSR effect in the very last cell of the arc.

It is worthwhile noticing here that the uncorrelated sum of initial emittance and CSR emittance in each DBA cell, depicted by Eq.8, may over-estimate, after several CSR kicks along the whole beamline, the final emittance growth. In fact, CSR chromatic kicks are correlated along the bunch. As explained in the introduction of this article, that property allows partial or full cancellation of CSR emittance at the beamline's end, through proper balance of successive kicks. Such a balance (correlation) stays behind the prescription of linear superposition of the CSR chromatic kick and the particle's coordinate, at any kick location. Hence, following [3], one should compute the evolution of the particle's coordinates throughout the entire beamline, and eventually calculate the C-S invariant; this will be coding both the information on the Twiss functions and the CSR kicks. This is actually what we did for formulating Eq.4, and, in order to be more rigorous, we should have continued following the invariant expression till the end of the arc. In that case, we would have found an expression for the final emittance of the same form of Eq.8, but with an optics coefficient that would allow partial cancellation of CSR emittance, as provided by the algebraic sum of successive CSR kicks along the arc, each of them properly "weighted" by the local bunch length (i.e., compression factor) and Twiss parameters. Eq.8, instead, shows no possibility of cancellation (although partial) when moving from one DBA cell to the next one.

Still it shows, like in the more general formulation of optics balance [3], that the CSR contribution to emittance growth is proportional to the unperturbed emittance (see the second term under square root in Eq.8). This property can be understood, for example, by interpreting the result of a CSR chromatic kick like a residual betatron oscillation around a new dispersive trajectory. If, however, beam has ideally no emittance at the line's entrance, namely particles do not perform betatron oscillations, the CSR kick would only translate the beam on a new trajectory, with null betatron amplitude (see also the Appendix and Fig.5 in [11]). This way, the beam emittance would remain null after the kick. The same property implies that, for CSR emittance much smaller than the initial emittance, namely $\gamma_i J_i << \varepsilon_{n,i-1}$, the difference of final and initial emittance does not depend on the initial emittance value, i.e. $\Delta\varepsilon_{n,i} = \varepsilon_{n,i} - \varepsilon_{n,i-1} \approx \gamma_i J_i / 2$.

Table 1: Main beam and arc compressor parameters for the analysis reported in Fig.2.

Parameter	*Value*	*Units*
Energy	2.4	GeV
Charge	0.5	nC
Initial Bunch Length, RMS	900	μm
Initial Peak Current	45	A
Correlated Energy Spread, RMS	0.4	%
R_{56} per DBA Cell	35	mm
Number of DBA Cells	6	
Total Compression Factor	45	
Final Peak Current	2000	A

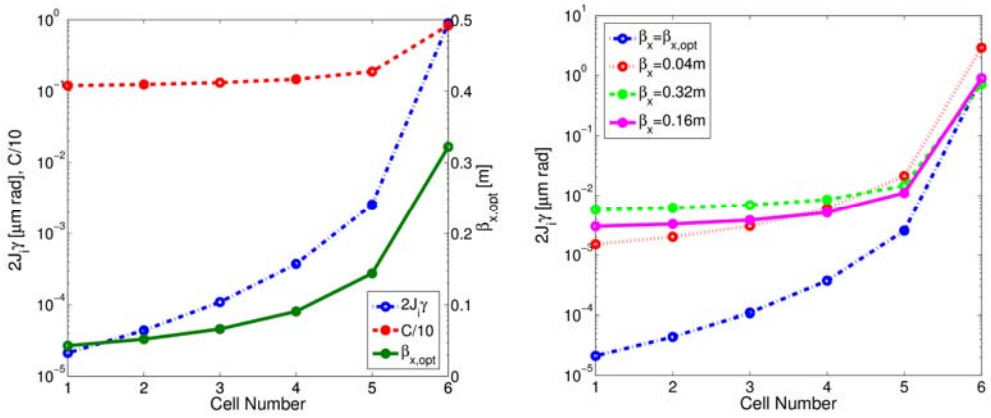

Figure 2: left, local value of the linear compression factor (normalized to 10; see Eq.7), and of the β_x-minimized CSR emittance (see Eq.4), along the arc; on the right axis, $\beta_{x,opt}$ in each cell predicted by Eq.6. Right, the local value of the β_x-minimized CSR emittance along the arc (dashed-dot line) is compared with its value evaluated for an identical β_x value in all the dipoles (3 cases are shown). Both left and right plots assume the electron beam parameters listed in Tab.1, and a CSR-induced relative energy spread of 2.5×10^{-6} in the first dipole of the arc. Copyright of Elsevier [2].

2.8.3 **Particle Tracking**

2.8.3.1 ***Emittance Dependence on Optics Functions, Charge and Energy***

The dependence of the final horizontal emittance on the optics, charge and mean energy is investigated through Elegant [12] particle tracking runs, and compared with analytical predictions based on the linear optics analysis. Beam and arc parameters used for these studies are listed in Tab.2. Figure 3 shows the behaviour of the final projected emittance as a function of the betatron function in the dipole magnets (both intended in the bending plane), respectively with (*enx_csr*) and without CSR (*enx_chrom*), at different beam charges. The minimum value of β_x in the dipoles is scanned by varying the strength of a family of quadrupole magnets external to the DBAs (Q1 in Fig.1); the beam is matched to the periodic optics solution at every step. Since the initial bunch

length and the total compression factor are kept fixed at different charges, the final peak current is different: it is 0.4 kA for 0.1 nC and approximately 4 kA at 1 nC. The initial emittance is also kept the same, for direct comparison of its value at the arc's end.

Table 2: Electron beam and arc compressor parameters for sensitivity studies. The set of beam parameters used in particle tracking runs does not necessarily reflect an optimized beam from the injector.

Parameter	***Value***	***Units***
Charge	0.1 / 1.0	nC
Mean Energy	0.5 – 2.4	GeV
Initial Bunch Length, FWHM	3	mm
Linear Energy Chirp	-4.7	m^{-1}
Initial Normalized Emittance, RMS	0.8(x), 0.8(y)	μm
R_{56} per DBA cell	35	mm
Number of DBA Cells	6	
Total Compression Factor	45	

When the optics is varied, the sextupole strengths (see Fig.1) are kept fixed, and thereby aberrations are not cancelled at each step. At this stage, however, we care of the CSR emittance only, which is proportional to the difference between *enx_chrom* and *enx_csr*. At 0.1 nC, the CSR effect is negligible over the entire range of β_x considered; the emittance growth is dominated by chromatic aberrations. The CSR effect is notable at 1.0 nC. The effect is minimum at $\beta_x \cong 0.26$ m, which is in between the theoretical optimum for the last but one and the very last cell (see also Fig.2-left plot). One can notice that similar values of β_x correspond in some cases to slightly different CSR emittance contributions: this is because when a new optics solution is found, the value of α_x also changes in the dipoles, thereby providing a different CSR emittance as depicted by Eq.4. There is a clear correlation between β_x and the final emittance value. It is a remarkable result that smallest β_x value does not lead to optimum suppression of the CSR effect, in agreement with the analytical and somehow counterintuitive prediction of Eq.4.

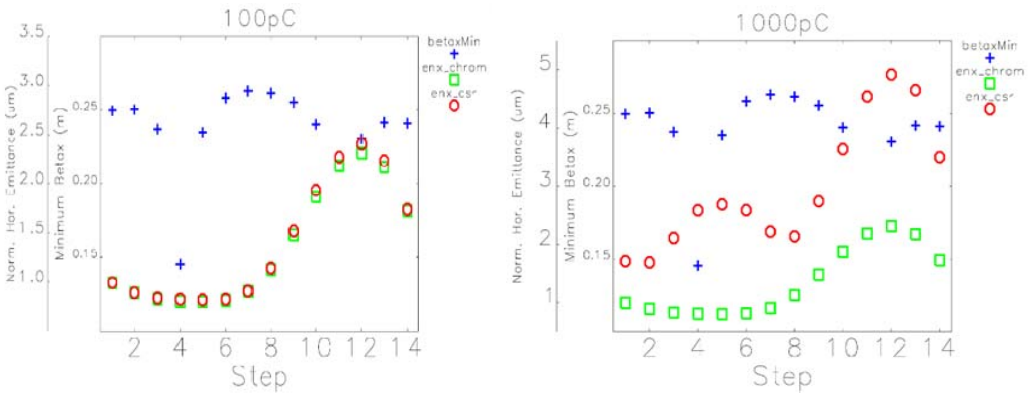

Figure 3: Horizontal normalized projected emittance (rms value) and minimum betatron function in the arc dipoles, at different simulation steps. Each step corresponds to a different periodic optics along the arc (Q1 strength is varied, see Fig.2). Bunch charge is 0.1 nC (left) and 1.0 nC; all other beam parameters are fixed (see Tab.2). Emittance is computed with (*enx_csr*) and without CSR (*enx_chrom*). Optical aberrations up to, and including 3rd order, and incoherent synchrotron radiation are always included. CSR transient field at the dipoles' edges and in drift sections following the dipole magnets is included when CSR is turned on. Copyright of Elsevier [2].

The arc compressor has also been investigated for different beam mean energies, as shown in Fig.4. The magnets' normalized strengths are kept fixed in order to provide the same optics for all energies. The quadratic difference of the final projected emittance and the initial unperturbed one is shown, for beam charges of 0.1, 0.3 and 0.5 nC. Particle tracking results are compared with the analytical prediction of Eq.8. CSR emittance control at 0.1 μm rad level is allowed at any energy $E \geq 0.5$ GeV for 0.1 nC, at $E \geq 1$ GeV for 0.3 nC, and at $E > 2$ GeV for 0.5 nC. It is worth noticing that the magnets' length and therefore the entire lattice was optimized for the maximum beam energy of 2.4 GeV, which is the maximum energy considered in our study. This implies that shorter magnets could be used at lower energies, and shorter drift sections accordingly. Thus, we envisage room for optimization of the lattice at lower energies that will provide a CSR emittance smaller than that shown in Fig.4. For the analytical case, the CSR-induced energy spread was evaluated according to the steady-state emission of a uniform charge distribution, as predicted by [8]. That value reasonably matches all simulation results, and is supported by a parabolic current profile which is used in the simulations (not shown).

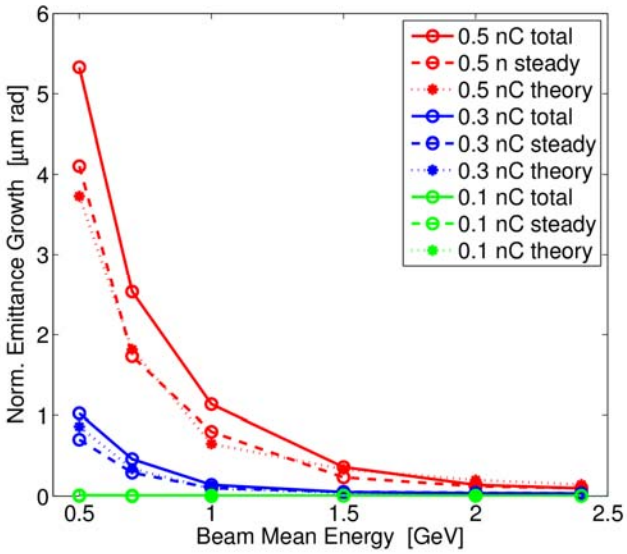

Figure 4: The normalized emittance growth is the quadratic difference (under square root) of the final projected normalized emittance and the initial one (rms values). Theoretical predictions (dotted lines) are from Eq.8, for steady-state CSR emission. Particle tracking results are for steady-state emission (dashed lines), and including transient CSR field at the dipoles' edges, and in drift sections (solid lines). The arc lattice is made of 6 consecutive cells, whose unit is shown in Fig.1. The optics is the same for all beam charges and energies. Copyright of Elsevier [1].

2.8.3.2 *Low and High Charge Beams*

A characterization of the electron distribution at the arc's end is provided here for two sets of initial beam parameters, one for high charge – long bunch, the other for low charge – short bunch; they are summarized in Tab.3. The high charge case is recalled from [1] for Reader's convenience, and for immediate comparison with the low charge. The bunch length compression process is linearized through the arc with the help of 4 families of sextupole magnets, 24 magnets in total (see Fig.1). In fact, linear compression is achieved as long as $|T_{566}|\sigma_{\delta,0} << |R_{56}|$ through the arc, whereas T_{566} is proportional to the second order momentum compaction. In addition, second and higher order energy chirp has to be small with respect to the linear one. While T_{566} can be controlled, *e.g.*, with an appropriate number and strength of sextupole magnets [13–15], a nonlinear energy chirp is realistically present in the beam's longitudinal phase space: at the entrance of the arc compressor due to upstream RF curvature, and developing along the arc because of the nonlinear energy correlation established by CSR along the bunch. Then, a non-zero T_{566} can be used to linearize the nonlinear chirp [13], the actual value of T_{566} (typically in the cm range) depending on the specific charge distribution. Magnetic linearization of the compression process has the advantage of avoiding the need for an RF harmonic linearizer [16]. However, it introduces a potential disruption of the beam rms emittance by geometric and chromatic aberrations induced by the sextupoles themselves. The single magnet aberration can be analytically estimated through the sigma matrix formalism, whose determinant, under square root, is the rms beam emittance. We assume that each magnet adds an error angular kick, $\Delta u'$, to the beam angular divergence. The beam geometric emittance after the kick reads:

$$\varepsilon = \sqrt{\det\begin{pmatrix} \beta & -\alpha \\ -\alpha & \gamma + \dfrac{\langle \Delta u'^2 \rangle}{\varepsilon_0} \end{pmatrix}} = \sqrt{\varepsilon_0^2 \left(1 + \frac{\beta \langle \Delta u'^2 \rangle}{\varepsilon_0} \right)} \approx \varepsilon_0 + \frac{1}{2} \beta \langle \Delta u'^2 \rangle, \tag{9}$$

where ε_0 is the unperturbed emittance, all symbols refer to the same plane of motion; β and γ are here Twiss parameters. The sextupole aberration is excited by a kick $\langle \Delta u'^2 \rangle = (k_2 l_s)^2 \langle u^2 \rangle^2$, with $k_2 l_s$ the integrated normalized sextupole strength in m^{-2}, $\langle u^2 \rangle = \beta \varepsilon_0$ for the geometric aberration, and $\langle u^2 \rangle = \eta_x^2 \sigma_\delta^2$ for the chromatic one. We consider the scenario in which the final relative emittance growth is given by the largest sextupole's contribution folded by the square root of the number of sextupoles in the lattice. With the beam parameters listed in Tab.3 for the 0.5 nC charge beam, and the optics depicted in Fig.1, we have at the sextupoles' location: $k_2 l_s \leq 8$ m^{-2}, $\beta\varepsilon_0 \leq 2 \times 10^{-9}$ m^2, and $(\eta_x \sigma_\delta)^2 \leq 1.4 \times 10^{-6}$ m^2. The total relative emittance growth from geometric aberrations is than smaller than 0.01%, while that due to chromatic aberrations is above 100%. That explains the modulation of the projected emittance along the arc shown in Fig.5.

The effect of chromatic aberrations was eventually minimzed by a numerical optimization of the sextupole strengths, and by profiting of the betatron phase advance between the magnets. As a result, the rms normalized projected emittance of the 0.5 nC beam grows from 0.8 μm rad to 1.1 μm rad at the arc's end, with residual contributions from incoherent synchrotron radiation (ISR), chromatic aberrations and CSR. Chromatic aberrations are also responsible for (small) horizontal slice emittance growth shown in Fig.6-left plot. Non-uniformity of the horizontal C-S invariant of the slices' centroid, shown in Fig.6-right plot, reflects the slices' misalignment in the transverse phase space due to CSR kicks. In order to damp the CSR-induced microbunching instability [17–19], the initial electron beam uncorrelated energy spread is set at 40 keV rms, in order to simulate the effect of a laser heater [20]. Quiet start of a 5 million particle input distribution, and filtering was adopted to ensure suppression of numerical sampling noise at uncompressed wavelengths shorter than 35 μm [21]. Residual CSR-induced microbunching shows up in the longitudinal phase space at compressed wavelengths longer than 10 μm. The final slice energy spread is approximately 2 MeV, and dominated by the initial uncorrelated energy spread times the total compression factor. Similar performances were obtained with the 0.1 nC beam, as shown in Fig.5-right plot and in Fig.7. The CSR-induced emittance growth is at same 0.1 μm rad level as in the 0.5 nC case, in agreement with Eq.8 and with the scaling of CSR effect with charge and bunch length [8]. Residual CSR-induced microbunching at final wavelengths longer than 5 μm is barely visible in Fig.7.

The 1-D steady-state theory of CSR emission from a Gaussian bunch allows an estimation of the CSR-induced mean energy loss per dipole magnet [22], $\langle \delta_{CSR} \rangle = -0.3505 r_e Q / (e \gamma \rho^{2/3} \sigma_z^{4/3})$. A more realistic evaluation from particle tracking included the energy loss associated to the electrons-field interaction in drift regions. We found that the 0.5 nC charge beam at 2.4 GeV (see Tab.3) emits along the whole arc, at a repetition rate of 1 MHz, an average coherent synchrotron radiation power of up to 6 kW, that is 12 kW per mA or 50 W per meter. The average power associated the classical synchrotron radiation emission amounts to 130 W, i.e. 260 W per mA or 1.1 W per

meter. That power can produce some relevant heating and therefore requires cooling and a careful evaluation of the machine run duration to prevent vacuum pressure rise.

Table 3: Electron beam parameters at the entrance and at the exit of the arc compressor (simulation results). Rms values are computed over 100% of the beam charge.

Input beam			
Energy	2.4	2.4	GeV
Charge	0.1	0.5	nC
Bunch Length, RMS	300	900	μm
Peak Current	30	45	A
Projected Normalized Emittance, RMS (x,y)	0.2, 0.2	0.8, 0.8	μm rad
Uncorrelated Energy Spread, RMS	30	40	keV
Correlated Energy Spread, RMS	0.1	0.4	%
Output beam			
Compression Factor	~45	~45	
Peak Current	~1400	~2000	A
Projected Normalized Emittance, RMS (x,y)	0.3, 0.2	1.1, 0.8	μm rad
Slice Energy Spread, RMS	≤1.6	≤2.0	MeV

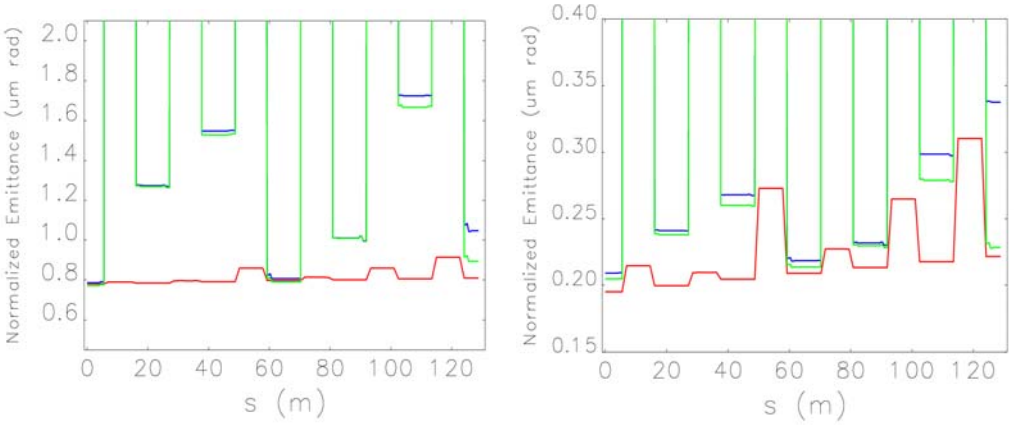

Figure 5: Projected normalized emittance (rms value) in the bending plane along the arc, for the 0.5 nC (left) and 0.1 nC beam (see Tab.3; notice that the vertical scale is different in the two plots). The emittance evolution is shown, respectively, in the presence of ISR-only for the fully compressed beam (red), with the addition of compression and optical aberrations (green) and with the further addition of CSR (blue). Upper value of the emittance along the arc is ~10 μm, not shown to appreciate the small emittance growth at the end of the line. Left plot is Copyright of Europhysics Letters [1]. Right plot is Copyright of Elsevier [2].

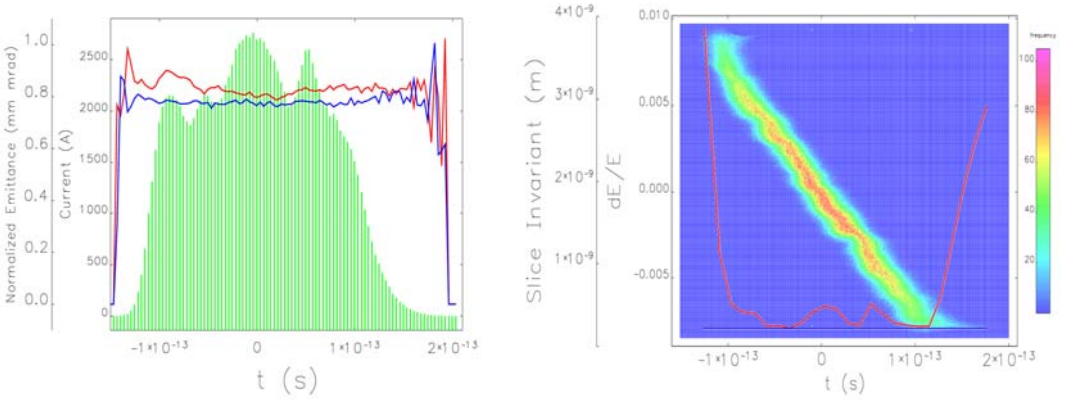

Figure 6: output from Elegant particle tracking for the 0.5 nC beam (see Tab.3). Bunch head is at negative time coordinates. Left: current profile (histogram), superimposed to the slice rms normalized emittance (horizontal, in red). Right: longitudinal phase space, superimposed to the slice C-S invariant (solid line): the horizontal one varies along the bunch because of CSR kicks. In both plots, spiky variations of the slice parameters at the bunch edges are due to poor particle sampling. Both plots are Copyright of Europhysics Letters [1].

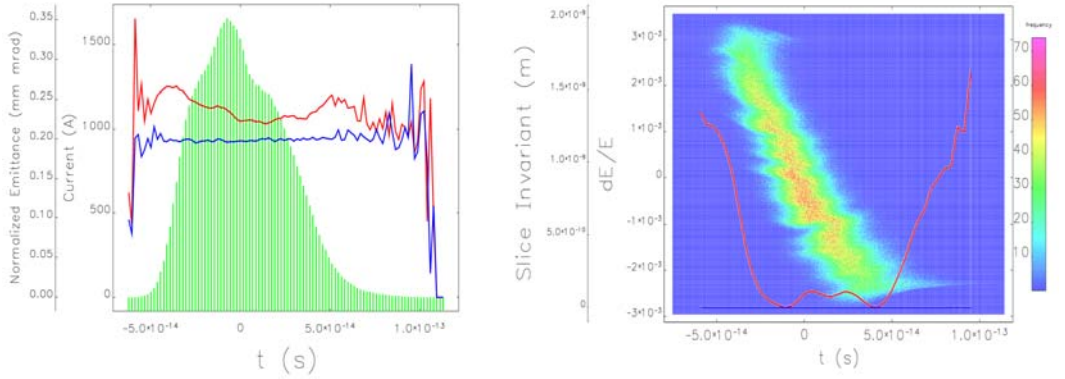

Figure 7: Output from Elegant particle tracking for the 0.1 nC beam (see Tab.3). Contents as in Fig.6. Both plots are Copyright of Elsevier [2].

2.8.4 **Applications**

The capability of controlling CSR effects in an arc compressor (not necessarily constrained to a 180 deg total bending angle) – and thus to increase the beam peak current while preserving its 6-D brightness using an approach that goes beyond those offered by the existing literature [23] – quite generally opens the door to new geometries in accelerator design and new schemes of beam longitudinal gymnastic. For example, after single- or multi-pass acceleration in an FEL linac-driver, the beam can be arc-compressed at high energy and counter-propagated into an undulator, which could then lie parallel to the accelerator. At least two advantages are seen: one is that cost savings are achieved in civil construction, the other is that the operation of the system is simplified, as much as the beam does not undergo any manipulation other than acceleration until it reaches the arc compressor. A similar layout may also apply to linear particle colliders. As an example, the CLIC design [24] includes optics matching insertions and a magnetic chicane both devoted to bunch length compression before an

isochronous turnaround arc, and a similar configuration (two chicanes aside an arc) is before beam deceleration. On the basis of our findings, the arc could be investigated as either compressor (together with a proper setting of the upstream RF phases to match the arc's positive R_{56}) or a CSR-immune transfer line, if the beam has no energy chirp at its entrance. A similar option might apply to the International Linear Collider, which is currently planning an isochronous turnaround followed by two compressor chicanes [25].

Our arc compressor design is also recommended for an ERL-, or recirculated linac-driven FEL such as that described in [26]. In this case, the electron beam may be accelerated and recirculated in isochronous beam lines until it reaches the target energy and energy chirp, and eventually compressed. From the entrance to the exit of the arc compressor, the energy spread, normally dominated by the energy chirp, remains substantially unchanged. In order for the FEL amplification process to be efficient, $\sigma_{\delta,0}$ must be matched to the normalized FEL energy bandwidth, ρ [27]. For lasing in x-rays, $\rho \geq 10^{-4}$ and this may require a removal of the energy chirp downstream of the arc, i.e. with a dedicated RF section. With the 500 pC beam parameters of Tab.1, we estimate [28] lasing at 1.3 nm with 2.1 m long 3-D gain length, $\rho = 1.1\times 10^{-3}$ and FEL power saturating at 2.6 GW in a 36 m long undulator.

If the incoming energy chirp is imposed to the beam at full energy with a linac running close to the zero-crossing RF phase, some concerns could be raised about the shot-to-shot jitter of the final beam energy, energy chirp and peak current, i.e. compression factor. It is shown below that such concerns are not justified when, e.g., stabilities typical of superconducting linacs are met. In the approximation of linear compression and for C>>1, the relative variation of C is linearly proportional to the relative variations of R_{56} and h, times C. In a periodic arc made of N DBAs we have:

$$R_{56} = N\int_0^{l_b} \frac{\eta_x(s)}{\rho} ds = N\int_0^{\theta} \rho(1-\cos\theta')d\theta' = 2Nl_b\left(1-\frac{\sin\theta}{\theta}\right) \propto \theta^2 \qquad (11)$$

Hence, we may estimate, $\Delta R_{56}/R_{56} = 2\Delta\theta/\theta \leq 2\times 10^{-4}$ where the bending angle relative stability is the same as the dipole magnetic field relative stability, and all dipoles are powered by the same current source. At the same time, the energy chirp $h \approx k_{RF}eV\cos(\phi)/E$ for $\phi \to 0$, with k_{RF} the RF wave number, V the RF peak voltage of the linac section imposing the energy chirp, ϕ the RF phase and E_i the beam mean energy at the linac entrance (maximum acceleration is for ϕ=90 deg). From this we get: $(\Delta h/h)_V \approx \Delta\phi tg(\phi) \leq 3\times 10^{-4}$ for RF set point $|\phi| < 20$ deg and RF phase jitter $\Delta\phi \approx$ 0.05 deg, and $(\Delta h/h)_\phi \approx \Delta V/V \leq 1\times 10^{-4}$. The uncorrelated sum of the jitters due to magnetic field, RF phase and RF peak voltage results in a peak current jitter smaller than 2% for C = 45. The beam mean energy jitter in the linac-chirper is also small, 0.02% rms at 2.4 GeV. This is equivalent to an arrival time jitter of 150 fs rms at the L-band linac entrance.

2.8.5 **Conclusions**

We have shown that linear optics transfer matrices associated to 1-D steady-state theory of CSR emission allow an estimation of projected emittance dilution due to CSR kicks in a periodic, achromatic, 180 deg arc compressor. The agreement with Elegant simulation results is at the level of 0.1 μm rad total normalized emittance growth (rms

value) for bunch charges lower than 0.5 nC. Above such a value, that accuracy is ensured at energies higher than 1.5 GeV. Our study shows a clear correlation between the optics design and the emittance value. As predicted by theory, a too small value of the betatron function in the arc's dipoles does not lead to optimum CSR suppression; an optimum betatron function is prescribed instead, and the overall CSR effect is minimized by optimum optics tuning in the very last cells of the arc. The theoretical background was eventually used to design a compressor arc largely immune to CSR-induced emittance growth.

Because of intrinsic higher order optics terms in the magnetic lattice and in the beam longitudinal phase space, sextupole magnets turned out to be essential to restore the linearity both of the optics and of the bunch length compression process. After an initial manual set up of the sextupoles' strengths in order to approach a compression as linear as possible, they were later on numerically optimized in order to minimize the final projected emittance. The last step ensured not only minimization of the optical aberrations, but also a linear longitudinal phase space because, as opposite, nonlinearities in the phase space would have led to current spikes, thus to larger CSR emittance.

Although CSR-induced microbunching shows up with a deeper modulation of the longitudinal phase space and a final current modulation around 20%, those tracking results should be considered as pessimistic estimates of the real beam quality: first, the smearing effect of transverse emittance on the microbunching, which may be particularly important as the bunch shortens in the last DBA cells, is ignored; second, the effect of numerical noise gradually diminishes as the number of particles is increased from 10^5 to $5\cdot 10^6$ (not shown); in addition, we have suppressed numerical noise at final wavelengths shorter than 1 μm, a value much shorter than those at which the instability develops (>5 μm). Finally, further optimization of the arc lattice with shorter drift sections and shorter dipole magnets is expected to reduce the CSR-induced microbunching.

The agreement of theory and simulations on the CSR-perturbed transverse emittance promises further reduction of the transverse CSR effect for smaller compression factors and/or improved tuning of the beam size in the dipole magnets. The optics that minimizes the transverse CSR effect in the arc is typically in conflict with the one cancelling chromatic effects, in analogy with the conflict of low emittance optics and chromaticity correction in storage rings. This fact leaves room for numerical optimization of both the arc lattice and its optics functions. Asymmetric arc designs with different optics arrangement can alternatively be considered [29], but we find that the periodic solution has several advantages: for example, energy dispersion leakage is easier to suppress if the dipole magnets are all identical and the optics is periodic. Optics symmetry allows tuning of the momentum compaction, thus of the compression factor, with equally spaced sub-families of quadrupoles (two families are available in the present design) and tune splitting to suppress coupling error effects ($\nu_x = 7.82$, $\nu_y = 3.41$ for the proposed arc). It also allows fast check of beam optics matching with screen systems along the line, as the beam sizes is the same at equivalent locations in the DBAs. Finally, periodicity of the lattice geometry allows cost-saving production of identical lattice elements (magnets, power supplies, diagnostics, etc.).

In conclusion, in spite of non-negligible non-steady state CSR effects, the present analysis can be used as a guidance for the design of a periodic and symmetric arc compressor in the presence of CSR, naturally further improved by numerical

optimization algorithms, and possibly modelling 3-D CSR effects. It is worth noticing that the CSR 1-D model in Elegant assumes that the bunch transverse size is much smaller than the bunch length. This requirement is often named "Derbenev criterion" and written in the form $\kappa = \sigma_x / \left(\rho \sigma_z^2\right)^{1/3} << 1$ [30]. In our case, the horizontal beam size in the dipoles is enlarged and dominated by the dispersive motion, and the criterion starts falling short already at the middle of the arc, where we have $\kappa \approx 0.1$; in the final cell we find $\kappa = 0.4$.

The proposed lattice, although not fully optimized for any specific application, promises an out coming electron beam quality at a level suitable for FELs in the ultra-violet to x-ray wavelength range. Similar electron beam parameters are of concern in nowadays linear collider projects.

2.8.6 **Acknowledgments**

This work took advantage of several stimulating discussions with, and suggestions by, colleagues in the accelerator community: M. Cornacchia, D. Douglas, Y. Jiao, X. Huang, M. Venturini, V. Litvinenko, D. Pellegrini, and A. Latina. This work was funded by the FERMI project and by the ODAC project of Elettra Sincrotrone Trieste.

2.8.7 **References**

1. S. Di Mitri and M. Cornacchia, Europhys. Letters **109**, 62002 (2015).
2. S. Di Mitri, "Feasibility Study of an Arc Compressor in the Presence of Coherent Synchrotron Radiation", accepted in Nucl. Instrum. Meth. Phys. Res., Vol. A (2015).
3. S. Di Mitri, M. Cornacchia, and S. Spampinati, Phys. Rev. Letters **110**, 014801 (2013).
4. R. Li, Ya.S. Derbenev, JLAB-TN-02-054 (2002).
5. J.S. Nodvick and D. Saxon, Phys. Rev. **96** (1954) 1.
6. V. Yakimenko, M. Fedurin, V. Litvinenko, A. Fedotov, D. Kayran, and P. Muggli, Phys. Rev. Lett. **109**, 164802 (2012).
7. Y. Jiao, X. Cui, X. Huang, G. Xu, Phys. Rev. Special Topics – Accel. Beams **17**, 060701 (2014).
8. E.L. Saldin, E.A. Schneidmiller, M.V. Yurkov, Nucl. Instrum. Meth. Phys. Research, Sect. A **398** (1997) 373.
9. A. Jackson, Part. Accel. 1987, 22, 111.
10. A.W. Chao and M. Tigner, *Handbook of Accelerator Physics and Engineering*, World Scientific, Singapore, 3rd ed. (2006) 66.
11. M. Venturini, "Design of a triple-bend isochronous achromat with minimum CSR-induced emittance growth", to be published (2015).
12. M. Borland, Advanced Photon Source LS-287 (2000).
13. D. Dowell, in Proc. of the 1997 Part. Accel. Conf., Vancouver, B.C., Canada (1997) 1888.
14. D. Douglas, in Proc. of the 2010 Beam Instrumentation Workshop, Santa Fe, NM, USA, WEIMNB02 (2010).
15. S. Thorin, M. Eriksson, S. Werin, D. Angal-Kalinin, J.W. McKenzie, B.L. Militsyn and P.H. Williams, in Proc. of the 32nd Intern. Free Electron Laser Conf., WEPB34, Malmö, Sweden (2010).
16. T. Smith, in Proc. of the 1984 Linear Accel. Conf., Stanford, CA, USA (1984), and in SLAC report 303 (1986).
17. E.L. Saldin, E.A. Schneidmiller, and M.V. Yurkov, Nucl. Instrum. Methods Phys. Res., Sect. A **490**, (2002) 1.

18. S. Heifets, S. Krinsky, G. Stupakov, Phys. Rev. Special Topics – Accel. Beams **5**, 064401 (2002).
19. Z. Huang and K.-J. Kim, Phys. Rev. Special Topics – Accel. Beams **5**, 074401 (2002).
20. E.L. Saldin, E.A. Schneidmiller, and M. Yurkov, Nucl. Instr. Meth. Phys. Research A **528** (2004) 355.
21. M. Borland, Phys. Rev. Special Topics – Accel. Beams **11**, 030701 (2008).
22. M. Borland, Phys. Rev. Special Topics – Accel. Beams **14**, 070701 (2001).
23. S. Di Mitri and M. Cornacchia, Physics Reports **539** (2014) 1–48.
24. CLIC Conceptual Design Report (2012), http://project-clic-cdr.web.cern.ch/project-CLIC-CDR/CDR_Volume1.pdf
25. C. Adoplphsen et al., Report No. CERN-ATS-2013-037 (2012), http://arxiv.org/ftp/arxiv/papers/1306/1306.6328.pdf
26. R.C. York, Phys. Rev. Special Topics – Accel. Beams **17**, 010705 (2014).
27. R. Bonifacio, C. Pellegrini and L. Narducci, Opt. Commun. 50, 373-378 (1984).
28. M. Xie, in Proc. of 1995 Part. Accel. Conf., Dallas, TX, USA, IEEE, 183–185 (1995).
29. D. Douglas et al., in Proc. of the 6th Intern. Part. Accel. Conf., TUPMA034, Richmond, VA, USA (2015), and references therein.
30. Ya.S. Derbenev, J. Rossbach, E.L. Saldin, and V.D. Shiltsev, TESLA-FEL 95-05 (1995), DESY, Hamburg, Germany.

2.9 Considerations of SRF Linac for High Current ERL

Wencan Xu, BNL, Upton, NY 11790
Mail to: wxu@bnl.gov

2.9.1 Introduction

The Collider-Accelerator Department at BNL proposed a FFAG lattice based electron-ion collider, eRHIC [1], which will use 80 5-cell 647 MHz SRF cavities for a 1.67 GeV main linac. The FFAG lattice based eRHIC design requires a SRF cavity design with capability of heavy damping HOMs, and keep high fundamental mode performance at the same time. The 5-cell 647 MHz BNL4 cavity is an evolution design of the 5-cell 704 MHz BNL3 cavity [3,4,5]. BNL4 was designed to reduce both loss factor of monopole HOMs (HOM power) and impedance of the dipole HOMs, while maintaining similar performance of the fundamental mode. The operation requirement of BNL4 cavity is 18.7 MV/m with Q_0 @ 3×10^{10}. A 5-cell prototype cavity is undergoing fabrication to demonstrate and study this performance. This paper addresses the design of BNL4 cavity.

To reach full luminosity of eRHIC at intermediate energies, about 7 kW HOM power per BNL4 cavity should be damped. It is a big challenge to develop such a high power, full spectrum HOM damping scheme. This paper will address the different HOM damping schemes that are studying at BNL. The goal is to develop a reliable, full HOM damping scheme for eRHIC and other high current ERL machines.